



Published in final edited form as:

J Med Chem. 2019 April 11; 62(7): 3286–3296. doi:10.1021/acs.jmedchem.8b01642.

Selective Inhibitors of *Helicobacter pylori* Methylthioadenosine Nucleosidase and Human Methylthioadenosine Phosphorylase

Rajesh K. Harijan[†], Oskar Hoff[‡], Rodrigo G. Ducati[†], Ross S. Firestone[†], Brett M. Hirsch[†], Gary B. Evans[‡], Vern L. Schramm^{*,†}, and Peter C. Tyler^{*,‡}

[†]Department of Biochemistry, Albert Einstein College of Medicine, New York 10461, New York, United States [‡]Ferrier Research Institute, Victoria University of Wellington, Wellington 5040, New Zealand

Abstract

Bacterial 5'-methylthioadenosine/*S*-adenosylhomocysteine nucleosidase (MTAN) hydrolyzes adenine from its substrates to form *S*-methyl-5-thioribose and *S*-ribosyl-*L*-homocysteine. MTANs are involved in quorum sensing, menaquinone synthesis, and 5'-methylthioadenosine recycling to *S*-adenosylmethionine. *Helicobacter pylori* uses MTAN in its unusual menaquinone pathway, making *H. pylori* MTAN a target for antibiotic development. Human 5'-methylthioadenosine phosphorylase (MTAP), a reported anticancer target, catalyzes phosphorolysis of 5'-methylthioadenosine to salvage *S*-adenosylmethionine. Transition-state analogues designed for *Hp*MTAN and MTAP show significant overlap in specificity. Fifteen unique transition-state analogues are described here and are used to explore inhibitor specificity. Several analogues of *Hp*MTAN bind in the picomolar range while inhibiting human MTAP with orders of magnitude weaker affinity. Structural analysis of *Hp*MTAN shows inhibitors extending through a hydrophobic channel to the protein surface. The more enclosed catalytic sites of human MTAP require the inhibitors to adopt a folded structure, displacing the phosphate nucleophile from the catalytic site.

Graphical Abstract

*Corresponding Authors: vern.schramm@einstein.yu.edu (V.L.S.), peter.tyler@vuw.ac.nz (P.C.T.).

Author Contributions

V.L.S. and P.C.T. supervised the project. O.H. synthesized the transition-state analogues. R.G.D., R.S.F., and B.M.H. expressed, purified the enzymes, and determined the enzyme kinetics. R.K.H. conducted the structure determinations and characterizations. R.K.H., R.G.D., P.C.T., and V.L.S. wrote the paper. All of the authors were involved in reviewing the data and manuscript drafts.

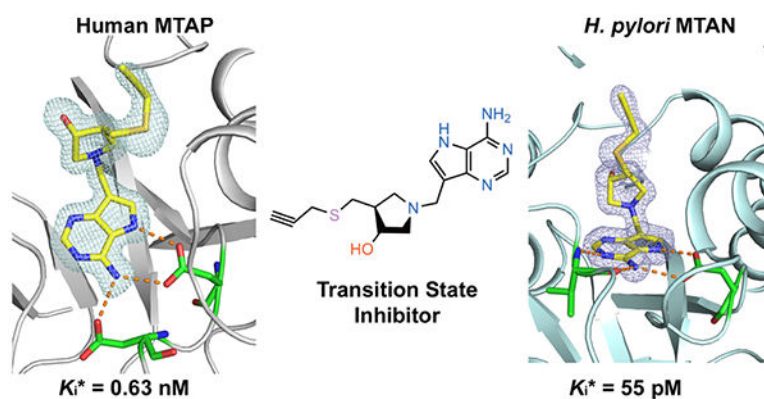
Supporting Information

The Supporting Information is available free of charge on the ACS Publications website at DOI: 10.1021/acs.jmedchem.8b01642. Title page and abbreviations; index to Supporting Information content; Figure S1, human MTAP subunit ribbon structure comparing free and liganded enzymes; Figure S2, electron density omit maps for MTAP–inhibitor complexes of **15**, **16**, **30**, **32**; Figure S3, inhibitor geometry at the catalytic sites of human MTAP and *Hp*MTAN; Figure S4, *Hp*MTAN subunit ribbon structures comparing free and liganded MTANs; Figure S5, electron density omit maps for *Hp*MTAN–inhibitor complexes of **15**, **16**, **30**, **32**; Table S1, crystallization and crystal handling; details of chemical synthesis; SMILES formula data for all inhibitions indexed by compound number; NMR spectra of all inhibitors (PDF)

Accession Codes

PDB ID CODES: 6DYZ, 6DZ0, 6DZ3, 6DZ2, 6DYU, 6DYV, 6DYY, 6DYW. The authors will release the atomic coordinates and experimental data upon article publication.

The authors declare no competing financial interest.



INTRODUCTION

S-Adenosylmethionine (SAM) is involved in biological methylation reactions, in polyamine biosynthesis, and as a precursor of glutathione.^{1,2} Two molecules of 5'-methylthioadenosine (MTA) are formed from SAM in the synthesis of each spermine molecule (Scheme 1). In humans, MTA is metabolized only by methylthioadenosine phosphorylase (MTAP) to form 5-methylthio- α -D-ribose 1-phosphate (MTR) and adenine. These are precursors for methionine and ATP, which can be recycled to SAM (Figure 1).^{3,4} Inhibition of MTAP in mammals causes elevated MTA and decreased recycling of MTA to SAM.^{5,6} Synthetic lethal genetic analysis of MTAP-deleted cancer cell lines indicates the sensitivity of these cell lines to pathways related to SAM-related methyl transfer.⁷⁻¹⁰ It has also been proposed that inhibitors of MTAP may have anticancer applications alone or in drug combinations, as they demonstrate anticancer properties in mouse xenograft models.^{5,6}

Most bacteria express methylthioadenosine/*S*-adenosylhomocysteine nucleosidase (MTAN) instead of MTAP. The enzyme hydrolyzes MTA and *S*-adenosylhomocysteine (SAH) to MTR or *S*-ribosylhomocysteine (SRH) and adenine, respectively (Scheme 1 and Figure 1). The MTAN reaction product, SRH, is used in the biosynthesis of homoserine lactones to form AI-2 quorum-sensing molecules.¹¹⁻¹³ MTAN is not essential in most bacteria, but a few species use the unusual futasine pathway for the biosynthesis of menaquinone, where MTAN plays an essential role.^{14,15} These organisms include the pathogens *Helicobacter pylori* and *Campylobacter jejuni*. Inhibition of this pathway is reported to be lethal to *H. pylori*.^{16,17} Inhibitors of MTAN are also expected to reduce polyamine biosynthesis and block the production of quorum-sensing autoinducer (AI-2) molecules. For these reasons, human MTAP and bacterial MTAN enzymes are of interest as drug targets.

Transition-state analogue enzyme inhibitors have the potential to bind orders of magnitude more tightly than substrates. Studies focused on *N*-ribosyltransferases have identified transition states with ribocation character.¹⁸ MTAP and MTAN share MTA as a substrate and form similar transition states, leading to similar interactions with transition-state analogues (Figure 1).¹⁹⁻²¹ MTAP inhibitors have shown efficacy in animal models against human tumors, whereas MTAN inhibitors influence bacterial quorum sensing and are antibiotics in organisms using the futasine pathway of menaquinone synthesis, notably, *H.*

pylori. We have reported transition-state analogues as inhibitors of human MTAP and several bacterial MTAN enzymes.^{16–26} Of several inhibitory chemical scaffolds, the DADMe-immucillin structure exemplified by MTDIA (**1**) is optimal for these enzymes (Scheme 1). Both enzymes tolerate substituents in the 4'-position of the 3'-hydroxypyrrolidine ring—in particular, for the bacterial MTAN enzymes. Here, we report on new analogues to explore the structure—activity relationships for human MTAP and *Hp*MTAN.

The transition-state structures of MTAN and MTAP enzymes have been solved by kinetic isotope effect measurements and quantum chemical calculations.^{19,21,27,28} Transition-state analogues for these enzyme.^{24–26} Two inhibitors, in particular, methylthio-DADMe-immucillin-A (MTDIA) and *para*chlorophenylthio-DADMe-immucillin-A (*p*Cl-PhT-DADMe-ImmA), were slow-onset inhibitors with dissociation constants (K_i^*) of 86 and 10 pM, respectively, for human MTAP and 86 and 570 pM, respectively, for *Hp*MTAN.^{17,22} Inhibitors reported here provide insight into the 4'-substituent inhibitor specificity for transition-state analogues of *Hp*MTAN and human MTAP.

RESULTS AND DISCUSSION

Synthesis of New Transition-State Analogue Inhibitors.

Modifications in the 9-Deazaadenine Moiety.—The N3 of **1** makes no catalytic site contacts in MTAP or MTAN enzymes, motivating the synthesis of a 3-deaza-analogue of **1**.^{17,23,29} Treatment of 2-hydroxy-4-methyl-3-nitropyridine (**2**) with Brederick's reagent afforded enamine **3** (Scheme 2), which with zinc in acetic acid gave 3,9-dideazahypoxanthine (**4**). This material was converted to 6-chloro-derivative **5**, which on treatment with catalytic copper(I) chloride in aqueous ammonia afforded 3,9-dideazaadenine (**6**). Mannich reaction of **6** and pyrrolidine **7** gave the desired 3-deazaMTDIA **8**.²²

During transition-state analogue design work for purine nucleoside phosphorylase, 8-aza-immucillins were found to be powerful inhibitors.^{26,30,31} The 8-aza-analogue of **1** was targeted for synthesis. Treatment of aldehyde **9**³² with pyrrolidine **7** and 2-methylpyridine borane complex gave **10** (Scheme 3). Ammonolysis followed by deprotection afforded 8-aza-MTDIA **11**.

Modifications in the 5'-Thio Substituent.—Both the human MTAP and *Hp*MTAN enzymes tolerate diversity in the 5'-thio substituents—particularly for the MTANs.²⁴ With this in mind, we prepared 5'-substituted thio-MTDIA analogues by coupling 5'-alkynyl derivatives with some azides using click chemistry.

Thioacetate **12**¹⁷ was treated with sodium methoxide/methanol followed by either propargyl bromide or 5-mesyloxy-pent-1-yne to give the alkynylthio-substituted compounds **13** and **14** (Scheme 4). These compounds, after acidic treatment to remove the Boc group followed by a Mannich reaction with 9-deazaadenine, then afforded **15** and **16**. Acetylenes **13** and **14** were individually treated with methyl iodide, allyl bromide, *n*-butyl bromide, or benzyl bromide along with sodium azide and catalytic copper(I) iodide affording the triazole “click” products **17–24**.³³ Deprotection followed by a Mannich reaction with 9-deazaadenine³⁴ then

provided the 5'-substituted thio-analogues **25–32**. 2-Pyrimidinethio analogue **33** was prepared by steps v, ii, and iii (Scheme 4).

Inhibition of MTAP and HpMTAN.—Most of the compounds described here are structurally related to methylthio-DADMeimmucillin-A (MTDIA), a transition-state analogue of MTAP and MTANs. Here, the varied 5'-alkylthio groups yielded strong inhibitors of MTAP and HpMTAN (Figure 2) with dissociation constants (K_d values) varying by over 2 orders of magnitude. Tight binding of these transition-state analogues depends on the ribocation mimic of the transition state provided by the cationic hydroxypyrrolidine and protonation of N7 in the 9-deazaadenine, a second important feature of the transition-state structure. The 6-amino group is essential, as its loss prevents binding (Figure 2).

Crystal Structures of Analogues with MTAP and HpMTAN.—Structural analysis of inhibitors **15**, **16**, **30**, and **32** bound to human MTAP and HpMTAN correlated the catalytic site interactions with the binding affinity to these enzymes (Figure 2 and Table 1). Human MTAP and HpMTAN were cocrystallized with the inhibitors and crystal structures solved by molecular replacement using PHASER at high resolutions (Table 1).³⁵ Structural analysis using MolProbity indicated that none of the amino acid residues are outliers in the Ramachandran plots (Table 1).³⁶

Human MTAP in complex with four inhibitors was solved at 1.62–1.99 Å resolutions in different space groups using the apo human MTAP monomer as the initial phasing model in PHASER. Human MTAP catalytic sites are located at the subunit interfaces of the trimer. Asymmetric units of human MTAP crystals contain a monomer with **15** and **16**, and a trimer with **30** and **32**. The trimer is the physiological state of human MTAP. Solvent accessible surface area of the subunit—subunit interfaces is 1187 Å². The low RMSD for C α (0.357–0.710 Å) of the four inhibitor-bound structures indicates only minor structural differences. MTAP monomers contain 10 β -sheets (residues are β 1, 11–16; β 2, 29–33; β 3, 45–50; β 4, 54–59; β 5, 87–98; β 6, 106–110; β 7, 112–116; β 8, 161–164; β 9, 165–172; β 10, 210–220) with 6 α -helices (from residues α 1, 73–84; α 2, 146–159; α 3, 180–189; α 4, 200–208; α 5, 233–259; α 6, 264–274; Figure S1). The electron density map of the peptide backbone and amino acid side chains are clearly resolved. Inhibitor binding is also well defined in the catalytic sites (Figure S2). The purine and pyrrolidine rings of the four inhibitors bind in the same conformation but the 5'-alkylthio group of **30** and **32** binds in a conformation different from **15** and **16** (Figure S3). The N1 of the inhibitor forms a hydrogen bond with a structural water molecule, whereas N6 forms hydrogen bonds with the carboxyl oxygens of both Asp220 and Asp222. Asp220 also forms a hydrogen bond interaction with N7, making it bidentate with respect to inhibitor binding. MTAP complexes of **15** and **16** have the hydroxyl groups and N1' (corresponding to the C1' of the substrate) of the pyrrolidine ring in hydrogen bond interactions with a phosphate oxygen and with Thr18 (Figure 3). The candidate nucleophilic oxygen (O2, nearest to the reaction center) of phosphate is hydrogen-bonded with Thr93 (OG1), Thr197 (OG1), and a water molecule. The O3 of the phosphate is in hydrogen bond interactions with peptide nitrogen of Thr18 and Ala94. Phosphate O4 forms hydrogen bonds with Arg60 (NH1) and His61 (NE2). These interactions are missing

in MTAP complexes with **30** and **32**, as phosphate is displaced in these structures. Instead, a chloride ion is bound near the phosphate binding pocket and is coordinated with Thr193 (OG1), Thr197 (OG1), and a water molecule. The 5'-alkylthio group binding mode of **15** and **16** is different from **30** and **32**, where the extended chain folds into the phosphate binding site (Figure 3 and Table 2).

*Hp*MTAN was cocrystallized with the same inhibitors and the structures solved at resolutions of 1.45–1.62 Å (Table 1). Previous and current analysis indicates a functional dimer for *Hp*MTAN. The solvent accessible surface area of the dimer interface is 1654 Å². *Hp*MTAN contains seven helices including one 3_{10} -helix and 10 β -sheets, similar to other MTAN structures.^{37–39} They are arranged in three $\alpha\beta\alpha$ -layer structures with central mixed β -sheets (Figure S4). The low RMSD (0.091–0.195 Å) of the inhibitor complexes indicates highly similar *C α* chains. Inhibitors were bound in both active sites of *Hp*MTAN with low B-factors and clear electron density maps (Figure S5). Except for the 5'-alkylthio groups, the binding modes of the inhibitors are similar (Figure S3). Inhibitors with extended 5'-alkylthio groups fill the full extent of the 5'-binding pocket, whereas short 5'-alkylthio groups do not. The binding modes of the purine and pyrrolidine rings of the inhibitors are the same. Hydrogen bond interactions to 9-deazaadenine include the Val154 nitrogen with N1, N6 with the carbonyl oxygen of Val154, and N7 with a carboxyl oxygen of Asp198 (OD2). N7 protonation is important to transition-state formation during the MTAN hydrolysis reaction. The structural nucleophilic water oxygen is 2.7 Å from N1', in hydrogen bond contacts with Glu13 (OE2) and Arg194 (NH1). The 3'-hydroxyl group of the pyrrolidine is hydrogen-bonded with a carboxyl oxygen of Glu175 (Figure 4). Inhibitor 5'-alkylthio groups occupy different parts of the 5'-alkylthio binding pocket, which extends toward the solvent exterior (Table 2 and Figure 4). Inhibitors **15** and **16** fill the 5'-alkylthio group binding pocket to engage most of the interactions with the enzyme.

Structural Comparisons.—Crystal structures of human MTAP with inhibitors **30** and **32** (large 5'-alkylthio groups) differ from those with **15** and **16** (smaller 5'-alkylthio groups). Binding of **30** and **32** caused rearrangement of the loop between β 1 and β 2 (residues 17–28) to a more open conformation than with **15** and **16** (Figure 5). In complex with **15** and **16**, this loop is closed. The rearrangement of the β 1– β 2 loop with **30** and **32** also alters the β 4– α 1 loop conformation and so His61 is displaced slightly and His65 is flipped 180°. The hydroxyl group of the pyrrolidine ring is rotated 18° toward the outside in **30** and **32** complexes. These conformational changes alter the phosphate binding site, which is occupied by the bulky 5'-alkylthio groups. For the structural comparisons, unliganded MTAP (PDB ID: 3OZE) and a complex with MTA and sulfate (PDB ID: 1CG6) were compared.^{40,41} These structures are similar to those with inhibitors **15** and **16**.

*Hp*MTAN structures with the same four inhibitors were solved at high resolution in the *P*4₁2₁2 space group (Table 1). In unliganded *E. coli* MTAN (PDB ID: 1Z5P), both catalytic sites are in an open configuration, but in unliganded *Hp*MTAN (PDB ID: 3NM4), the binding of a Tris buffer molecule induced a closed conformation in monomer-A with monomer-B in an open conformation.^{39,42,43} The ligand-induced conformation change moves the β 10– α 6 loop approximately 7 Å closer to the binding site to form the closed

state. When the *Hp*MTAN bound to **15**, **16**, **30**, and **32** was compared to *p*-CIPh-Thio-DADMe-ImmA bound to *Hp*MTAN and resolved with neutron diffraction (PDB ID: 5K1Z), hydrogen bond contacts of the DADMe-ImmA core were found to be intact, including the N7 hydrogen sharing with Asp198.⁴⁴ All *Hp*MTAN–inhibitor complexes are in closed configurations but differ in the 5′-alkylthio group binding pocket (Table 2; Figures 4 and 5).

Structure–Inhibition Relationship.—Inhibitors **15** and **16** gave K_d values of 0.63 and 0.94 nM, respectively, for human MTAP, slightly better than **30** and **32**, with K_d values of 1.3 and 1.4 nM, respectively. 9-Deazaadenine of the inhibitors is colocated in the catalytic site for the four inhibitors, whereas the 3′-hydroxyl group of the pyrrolidine of **30** and **32** is shifted upward relative to **15** and **16** (Figures S1 and S3). The 5′-alkylthio groups of the inhibitors, important for the potency, are bound in different conformations. Inhibitors **15** and **16** occupy the hydrophobic binding site normally occupied by the 5′-methylthio or 5′-homocysteinyloxy groups of the natural substrates. In contrast, **30** and **32** induced β 1– β 2 loop rearrangement by exceeding the size of the 5′-alkylthio binding pocket. Upon **30** and **32** binding, the inhibitor triazoles reposition under the 3′-hydroxypyrrolidine to occupy the phosphate binding site. As **30** and **32** occupy both nucleoside and phosphate binding sites, phosphate is not bound in the **30** and **32** MTAP complexes. Ion pair formation between the cationic 3′-hydroxypyrrolidine ring and anionic phosphate is part of the transition-state ensemble, contributing to tight binding of structurally compatible analogues. Remarkably, most of the binding affinity is retained in **30** and **32** without bound phosphate.

Enzyme inhibition experiments revealed that **15**, **16**, **30**, and **32** are 26–55 picomolar inhibitors of *Hp*MTAN (Figure 2). The 5′-alkylthio binding site accommodates groups approximately 10 Å, extending from the 4′-carbon of the pyrrolidine group, and longer groups are accommodated, as the binding channel opens toward the solvent. The optimal fit of **16** to the site explains its high binding affinity, but even relatively small 5′-alkylthio groups (**15**) or bulky and hydrophilic triazole groups (**30** and **32**) are picomolar inhibitors. In the *Hp*MTAN–**15** complex, the unfilled space in the 5′-alkylthio binding pocket is occupied by an ethylene glycol molecule interacting with solvent molecules and a carboxyl oxygen Asp209 (OD1). The groups of **30** and **32** are larger, forcing them into the solvent space beyond the organized binding site. The distal atoms of **30** and **32** are disordered, resulting in decreased affinity. Despite these differences, the sum of the interactions provides favorable binding energy (Table 2 and Figure 4).

Inhibitor catalytic site contacts in both *Hp*MTAN and MTAP show no interactions with the N3 atom of 9-deazaadenine. In contrast, both enzymes have hydrogen bond interactions with the protonated N7. As protonation of N7 is a feature of the transition state, this is an important characteristic of high-affinity inhibitors. A 3,9-dideazaadenine inhibitor (**8**) retains the desired protonation at N7 in a scaffold otherwise identical to MTDIA (**1**). However, (**1**) is an 86 pM inhibitor for both *Hp*MTAN and MTAP, whereas the dissociation constant for (**8**) increased by >100-fold to 10 and 32 nM for *Hp*MTAN and MTAP, respectively, indicating weaker N7 to enzyme interactions because of the loss of electron contribution from N3. The N6 exocyclic amino group is doubly hydrogen-bonded at the catalytic sites,

and its replacement by O6 eliminates binding to the catalytic sites, even at concentrations of 5 μM (**34** and **35**).

CONCLUSIONS

Human MTAP is a validated drug target. Its genetic deletion in 15% of all human cancers makes those malignancies more susceptible to inhibitors of PRMT5, MAT2A, or RIOK1.^{7–10} *HpMTAN* catalyzes an essential step in menaquinone synthesis in *H. pylori* but not in common gut bacteria, making it a species-specific target in the treatment of peptic ulcers. New transition-state analogues of *HpMTAN* and MTAP were synthesized to explore variations of the MT-DADMeimmucillin-A chemical scaffold and the structure-function relationship to these target enzymes. The 4'-position of the 3'-hydroxypyrrolidine ring of DADMe-immucillin-A was varied by the click chemistry addition of varied substituents. Inhibition constants indicated the best compounds (**15** and **16**) to be picomolar inhibitors against both MTAP and *HpMTAN*, with 12- to 36-fold preference for the *HpMTAN*. Bulky 4'-substituents (e.g., **25–29** and **33**) showed a 92- to 243-fold preference for *HpMTAN*. The hydrophobic pocket accepting the 4'-substituent in *HpMTAN* can accommodate methylthio (in MTA), homocysteine (in SAH), and the bulky side chain of aminofutalosine. It does so in a hydrophobic tunnel that opens toward the solvent. Human MTAP has a more restricted 4'-binding pocket that accepts only the methylthio and homocysteine groups. Larger substituents fold under the 3'-hydroxypyrrolidine ring and occupy the phosphate binding site while retaining other contacts to the 9-deazaadenine and hydroxypyrrolidine that dominate the transition-state binding energy. Four transition-state analogues were cocrystallized with MTAP and *HpMTAN*. Structural analysis revealed that the binding of **30** and **32** to human MTAP caused a structural rearrangement to displace phosphate and accommodate long and bulky 5'-alkylthio groups. With *HpMTAN*, inhibitor **16** takes full advantage of the *HpMTAN* binding pocket and thus binds more tightly than other inhibitors.

MATERIALS AND METHODS

Chemical Synthesis of Transition-State Analogues.

The MTDIA chemical scaffold was explored by synthesizing a new generation of transition-state analogues for *HpMTAN* and MTAP. The 4'-position of the 3'-hydroxypyrrolidine ring of MTDIA was varied by click chemistry. All reactions were performed under an argon or nitrogen atmosphere unless water was used as solvent or the reaction mixture was heated to above 100 °C. All final compounds gave satisfactory purity (>95%) by HPLC and by ¹H and ¹³C NMR spectroscopies. Details of the chemical synthesis are provided in the Supporting Information.

Expression and Purification of Human MTAP.

Human MTAP was prepared, as previously described with some modifications.⁴¹ In brief, a plasmid containing the coding region for MTAP was transformed into BL21-CodonPlus(DE3)-RIPL *E. coli* chemically competent cells. Nucleotide sequencing validated the DNA sequence for MTAP. The culture was grown at 37 °C and 200 rpm in LB medium containing 100 $\mu\text{g mL}^{-1}$ ampicillin. Heterologous protein expression was induced when

OD₆₀₀ reached 0.6–0.8 by the addition of 1 mM IPTG (final concentration). After 8 h induction at 37 °C and 200 rpm, the cells were harvested by centrifugation (5000g for 20 min) and stored at –80 °C. All subsequent steps were carried out at 4 °C unless stated otherwise.

The pellet was suspended in lysis buffer (50 mM HEPES–NaOH, 5 mM imidazole at pH 7.0) (2.5 mL g⁻¹ of cell pellet) with the addition of protease inhibitor cOmplete Mini EDTA-free (one tablet per 20 g of cell pellet; Roche) and homogenized by stirring for 30 min. A spatula tip of lysozyme (Sigma-Aldrich) and DNase I (Sigma-Aldrich) was added to the mixture and, after 30 min of stirring, cells were disrupted by sonication (15 s on, 15 s off, at 30% amplitude for 30 min) and centrifuged (20 000g for 20 min) to remove cell debris. The recombinant MTAP contains 14 additional amino acids at N-terminus of the native enzyme, including a His₆ tag (and a TEV protease cleavage site). The supernatant was incubated with Ni-NTA agarose (1.0 mL of slurry/g of cell pellet; Qiagen) for 45 min with rocking, and the mixture was poured into an empty column and washed with 12 column volumes of cell lysis buffer. The collection of 4 column volume fractions from a 50–500 mM imidazole stepwise elution gradient gave proteins analyzed by sodium dodecyl sulfate polyacrylamide gel electrophoresis (SDS-PAGE) (200 V and 185 mA for 60 min in MOPS running buffer) analysis, and the fractions containing the target protein with a purity of over 95% (150–500 mM imidazole) were pooled. Purified MTAP contains adenine, which was removed by dialysis against 50 mM HEPES–NaOH at pH 7.0 with 0.2% (m/v) activated charcoal (Sigma-Aldrich) overnight, using 10 kDa dialysis cassettes (Thermo Scientific). Adenine analysis in MTAP involved denaturation with 10% (v/v) perchloric acid. Denatured protein was removed by centrifugation, and the concentration of adenine in the supernatant was tested by spectrophotometry. Adenine-free MTAP was concentrated to approximately 300 μM or 10 mg mL⁻¹ (extinction coefficient is estimated to be 30.94 mM⁻¹ cm⁻¹ at 280 nm), and aliquots were frozen in liquid nitrogen and stored at –80 °C. A total of 21 mg of protein was obtained from 10 L of culture.

Expression and Purification of *HpMTAN*.

HpMTAN was prepared, as previously described with some modifications.^{16,17} Briefly, the plasmid-containing His-tag *HpMTAN* gene was transformed into BL21 (DE3) *E. coli* chemically competent cells. Nucleotide sequencing validated the DNA sequence for *HpMTAN*. The culture was grown at 37 °C and 200 rpm in LB medium containing 50 μg mL⁻¹ ampicillin, and heterologous protein expression was induced when OD₆₀₀ reached 0.6–0.8 by the addition of 0.5 mM IPTG (final concentration). Temperature was lowered to 30 °C upon the addition of IPTG, and the culture was grown for an additional 20 h. Cells were harvested by centrifugation (5000g for 20 min) and stored at –80 °C. All subsequent steps were carried out at 4 °C unless stated otherwise. The purification of *HpMTAN* was the same as described above for MTAP. A total of 210 mg of protein was obtained from 2 L of culture.

Inhibition Assays of MTAP.

MTAP catalytic activity was measured using the absorbance difference between MTA and adenine.⁴¹ A second assay followed the conversion of MTA to 2,8-dihydroxyadenine based

on the oxidation of adenine by xanthine oxidase to give an absorbance change at 305 nm ($\epsilon_{305} = 15.5 \text{ mM}^{-1} \text{ cm}^{-1}$). Inhibition constants were analyzed by fitting rate data to the Morrison quadratic equation.⁴⁵ Reactions in a 1 mL cuvette contained 100 mM K_2PO_4 , 1 mM DTT, 800 μM MTA, 3 nM MTAP, 1 unit of xanthine oxidase, and varying concentrations of each inhibitor. Equilibrium dissociation constants were determined from reaction rate inhibition following slow-onset binding (K_i^*). The rates of each reaction were taken 40 min after the initiation of the reaction, a time when slow-onset equilibrium had occurred.

Inhibition Assays of *Hp*MTAN.

Inhibition constants were determined as above. Reactions (1 mL) contained 100 mM HEPES pH 7.2, 1 mM DTT, 100 mM NaCl, 1 mM MTA, 0.6 nM *Hp*MTAN, 1 unit of xanthine oxidase, and varying concentrations of each inhibitor (0–100 μM). Reactions were monitored, as described above for MTAP to obtain the inhibition constants following slow-onset binding when appropriate (K_i^*). The rates of each reaction were taken 40 min after the initiation of the reaction, to a time when slow-onset equilibrium had occurred.

Cocrystallization with Transition-State Analogues.

Cocrystallization of MTAP and *Hp*MTAN with four tight binding transition-state analogues (**15**, **16**, **30**, and **32**) used sitting drop vapor diffusion at 22 °C. MTAP or *Hp*MTAN (5 mg mL^{-1}) was mixed with inhibitors in a 1:2 molar ratio and incubated for 2 h on ice. The proteins were screened for crystal-forming conditions with the Microlytic (MCSG1–4) and Hampton (crystal screenHT) kits. Crystallization trials were in 96-well INTELLI plates, using the CRYSTAL-GRYPHON crystallization robot (ART ROBBINS). Crystallization drops contained 0.5 μL of enzyme–inhibitor mixture and 0.5 μL of well solution. The volume of the well solution was 70 μL . Good-quality crystals were obtained in 1 week (Table 1).

Data Collection and Processing.

Diffraction data were collected at the LRL-CAT beamline (Argonne National Laboratory, Argonne, IL) at a wavelength of 0.97931 Å (Table 1). Data were processed using the iMOSFLM program and scaled by the AIMLESS program in the CCP4 suite, using the appropriate space group (Table 1).^{46,47} Data quality was analyzed using the SFCHECK and XTRIAGE.^{47,48} Matthews coefficient (V_m) calculations indicated the number of monomers present in the unit cells.

Structure Determination and Refinement.

Crystal structures of MTAP and *Hp*MTAN in complex with transition-state analogue inhibitors were solved by molecular replacement using PHASER.³⁵ Chain-A of wild-type MTAP (PDB ID: 5TC6) and *Hp*MTAN (PDB ID: 4WKP) structures was used as the initial phasing model. The model obtained from PHASER was manually adjusted and completed using the graphics program COOT.⁴⁹ Structure refinement was performed with REFMAC5, using standard protocols for the NCS refinement.⁵⁰ Inhibitor molecules were deleted from

the models to initiate the refinement. After water was added, inhibitor molecules were fitted into their electron densities (Table 1).

Structure Analysis.

Crystal structures of unliganded wild-type MTAP (PDB ID: 3OZE, chain: B), *Hp*MTAN (PDB ID: 3NM4, chain: B), and *Ec*MTAN (PDB ID: 1Z5P, chain: A) were used for structure comparisons. The MTA complex with MTAP (PDB ID: 3T94) and p-CIPh-Thio-DADMe-ImmA complex with *Hp*MTAN (PDB ID: 5K1Z) were also used in the structural comparisons. All structural superimpositions used the SSM protocol of COOT, and the geometry analyses of the final model used MolProbity.³⁶ Additional structure analyses, including the calculation of the B-factor profiles, used BAVERAGE of the CCP4 suite.⁴⁷ Structural figures were generated with the molecular graphics program PyMOL. For MTAP and *Hp*MTAN structures, subunit-A was used for all of the structural analyses and comparisons.

Supplementary Material

Refer to Web version on PubMed Central for supplementary material.

ACKNOWLEDGMENTS

This project was supported by research grant GM041916 from the National Institutes of Health and the New Zealand Foundation for Research Science and Technology contract C08X0701. The Albert Einstein Crystallographic Core X-ray diffraction facility is supported by NIH Shared Instrumentation Grant S10 OD020068. Data collection also involved resources of the Advanced Photon Source, a US Department of Energy (DOE) Office of Science User Facility operated for the DOE Office of Science by Argonne National Laboratory under Contract No. DE-AC02-06CH11357. Use of the Lilly Research Laboratories Collaborative Access Team (LRL CAT) beamline at Sector 31 of the Advanced Photon Source was provided by Eli Lilly Company, which operates the facility.

ABBREVIATIONS

MTDIA	methylthio-DADMe-immucillin-A
MTA	<i>S</i> -methyl-5'-thioadenosine
All	allyl
DQF-COSY	double-quantum filtered correlation spectroscopy
Q-TOF	quadrupole time-of-flight
MTAN	5'-methylthioadenosine/ <i>S</i> -adenosylhomocysteine nucleosidase
<i>Hp</i>MTAN	<i>Helicobacter pylori</i> MTAN
MTAP	5'-methylthioadenosine phosphorylase
MTR	5-methylthio- α -D-ribose 1-phosphate
SAM	<i>S</i> -adenosylmethio-nine
SAH	<i>S</i> -adenosylhomocysteine

SRH	S-ribosylhomocysteine
NMR	nuclear magnetic resonance
HPLC	high-performance liquid chromatography
RT	room temperature
<i>t</i>-Bu	<i>tert</i> -butyl
DMF	dimethylformamide
aq	aqueous
Et	ethyl
Me	methyl
THP	tetrahydropyranyl
BOC	<i>tert</i> -butyloxycarbonyl
Ac	acyl
<i>n</i>-Bu	<i>n</i> -butyl
Bn	benzyl
PRMT5	protein arginine methyltransferase 5
MAT2A	<i>S</i> -adenosylmethionine synthetase 2A
HSQC	heteronuclear single quantum coherence spectroscopy
DEPT	distortionless enhancement by polarization transfer
APT	attached proton test

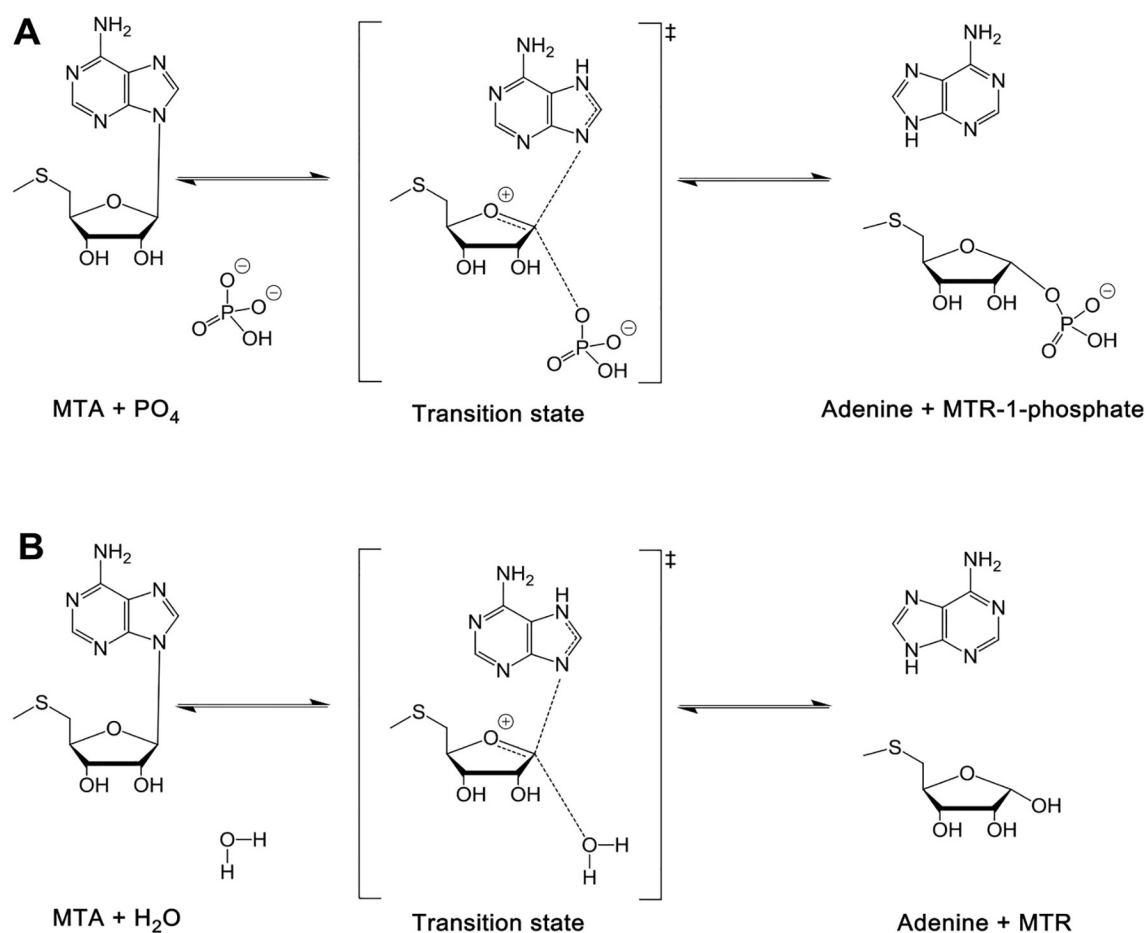
REFERENCES

- (1). Lieber CS; Packer L *S*-Adenosylmethionine: Molecular, Biological, and Clinical Aspects—an Introduction. *Am. J. Clin. Nutr* 2002, 76, 1148S–1150S. [PubMed: 12418492]
- (2). Loenen WAM *S*-Adenosylmethionine: Jack of All Trades and Master of Everything? *Biochem. Soc. Trans* 2006, 34, 330–333. [PubMed: 16545107]
- (3). Battaglia V; DeStefano Shields C; Murray-Stewart T; Casero RA Jr. Polyamine Catabolism in Carcinogenesis: Potential Targets for Chemotherapy and Chemoprevention. *Amino Acids* 2014, 46, 511–519. [PubMed: 23771789]
- (4). Tabor CW; Tabor H Polyamines. *Annu. Rev. Biochem* 1984, 53, 749–790. [PubMed: 6206782]
- (5). Basu I; Cordovano G; Das I; Belbin TJ; Guha C; Schramm VL A Transition State Analogue of 5'-Methylthioadenosine Phosphorylase Induces Apoptosis in Head and Neck Cancers. *J. Biol. Chem* 2007, 282, 21477–21486. [PubMed: 17548352]
- (6). Basu I; Locker J; Cassera MB; Belbin TJ; Merino EF; Dong X; Hemeon I; Evans GB; Guha C; Schramm VL Growth and Metastases of Human Lung Cancer Are Inhibited in Mouse Xenografts by a Transition State Analogue of 5'-Methylthioadenosine Phosphorylase. *J. Biol. Chem* 2011, 286, 4902–4911. [PubMed: 21135097]

- (7). Mavrakis KJ; McDonald ER 3rd; Schlabach MR; Billy E; Hoffman GR; deWeck A; Ruddy DA; Venkatesan K; Yu J; McAllister G; Stump M; deBeaumont R; Ho S; Yue Y; Liu Y; Yan-Neale Y; Yang G; Lin F; Yin H; Gao H; Kipp DR; Zhao S; McNamara JT; Sprague ER; Zheng B; Lin Y; Cho YS; Gu J; Crawford K; Ciccone D; Vitari AC; Lai A; Capka V; Hurov K; Porter JA; Tallarico J; Mickanin C; Lees E; Pagliarini R; Keen N; Schmelzle T; Hofmann F; Stegmeier F; Sellers WR Disordered Methionine Metabolism in MTAP/CDKN2A-Deleted Cancers Leads to Dependence on PRMT5. *Science* 2016, 351, 1208–1213. [PubMed: 26912361]
- (8). Kryukov GV; Wilson FH; Ruth JR; Paulk J; Tsherniak A; Marlow SE; Vazquez F; Weir BA; Fitzgerald ME; Tanaka M; Bielski CM; Scott JM; Dennis C; Cowley GS; Boehm JS; Root DE; Golub TR; Clish CB; Bradner JE; Hahn WC; Garraway LA MTAP Deletion Confers Enhanced Dependency on the PRMT5 Arginine Methyltransferase in Cancer Cells. *Science* 2016, 351, 1214–1218. [PubMed: 26912360]
- (9). Pfister SX; Ashworth A Marked for Death: Targeting Epigenetic Changes in Cancer. *Nat. Rev. Drug Discovery* 2017, 16, 241–263. [PubMed: 28280262]
- (10). Marjon K; Cameron MJ; Quang P; Clasquin MF; Mandley E; Kunii K; McVay M; Choe S; Kernysky A; Gross S; Konteatis Z; Murtie J; Blake ML; Travins J; Dorsch M; Biller SA; Marks KM MTAP Deletions in Cancer Create Vulnerability to Targeting of the MAT2A/PRMT5/RIOK1 Axis. *Cell Rep* 2016, 15, 574–587. [PubMed: 27068473]
- (11). Parveen N; Cornell KA Methylthioadenosine/S-Adenosylhomocysteine Nucleosidase, a Critical Enzyme for Bacterial Metabolism. *Mol. Microbiol* 2011, 79, 7–20. [PubMed: 21166890]
- (12). Chen X; Schauder S; Potier N; Van Dorsselaer A; Pelczar I; Bassler BL; Hughson FM Structural Identification of a Bacterial Quorum-Sensing Signal Containing Boron. *Nature* 2002, 415, 545–549. [PubMed: 11823863]
- (13). Xavier KB; Bassler BL LuxS Quorum Sensing: More than Just a Numbers Game. *Curr. Opin. Microbiol* 2003, 6, 191–197. [PubMed: 12732311]
- (14). Dairi T An alternative menaquinone biosynthetic pathway operating in microorganisms: an attractive target for drug discovery to pathogenic *Helicobacter* and *Chlamydia* strains. *J. Antibiot* 2009, 62, 347–352 [PubMed: 19557031]
- (15). Li X; Apel D; Gaynor EC; Tanner ME 5-methylthioadenosine nucleosidase is implicated in playing a key role in a modified futasoline pathway for menaquinone biosynthesis in *Campylobacter jejuni*. *J. Biol. Chem* 2011, 286, 19392–19398. [PubMed: 21489995]
- (16). Wang S; Haapalainen AM; Yan F; Du Q; Tyler PC; Evans GB; Rinaldo-Matthis A; Brown RL; Norris GE; Almo SC; Schramm VL A Picomolar Transition State Analogue Inhibitor of MTAN as a Specific Antibiotic for *Helicobacter pylori*. *Biochemistry* 2012, 51, 6892–6894. [PubMed: 22891633]
- (17). Wang S; Cameron SA; Clinch K; Evans GB; Wu Z; Schramm VL; Tyler PC New Antibiotic Candidates against *Helicobacter pylori*. *J. Am. Chem. Soc* 2015, 137, 14275–14280. [PubMed: 26494017]
- (18). Schramm VL Enzymatic Transition States, Transition-State Analogs, Dynamics, Thermodynamics, and Lifetimes. *Annu. Rev. Biochem* 2011, 80, 703–732. [PubMed: 21675920]
- (19). Singh V; Schramm VL Transition-State Structure of Human 5'-Methylthioadenosine Phosphorylase. *J. Am. Chem. Soc* 2006, 128, 14691–14696. [PubMed: 17090056]
- (20). Gutierrez JA; Luo M; Singh V; Li L; Brown RL; Norris GE; Evans GB; Furneaux RH; Tyler PC; Painter GF; Lenz DH; Schramm VL Picomolar Inhibitors as Transition-State Probes of 5'-Methylthioadenosine Nucleosidases. *ACS Chem. Biol* 2007, 2, 725–734. [PubMed: 18030989]
- (21). Singh V; Lee JE; Nunez S; Howell PL; Schramm VL Transition State Structure of 5'-Methylthioadenosine/S-Adenosylhomocysteine Nucleosidase from *Escherichia coli* and Its Similarity to Transition State Analogues. *Biochemistry* 2005, 44, 11647–11659. [PubMed: 16128565]
- (22). Evans GB; Furneaux RH; Lenz DH; Painter GF; Schramm VL; Singh V; Tyler PC Second Generation Transition State Analogue Inhibitors of Human 5'-Methylthioadenosine Phosphorylase. *J. Med. Chem* 2005, 48, 4679–4689. [PubMed: 16000004]

- (23). Haapalainen AM; Thomas K; Tyler PC; Evans GB; Almo SC; Schramm VL Salmonella enterica MTAN at 1.36 Å Resolution: A Structure-Based Design of Grouped Transition State Analogs. *Structure* 2013, 21, 963–974. [PubMed: 23685211]
- (24). Longshaw AI; Adanitsch F; Gutierrez JA; Evans GB; Tyler PC; Schramm VL Design and Synthesis of Potent “Sulfur-Free” Transition State Analogue Inhibitors of 5′-Methylthioadenosine Nucleosidase and 5′-Methylthioadenosine Phosphorylase. *J. Med. Chem* 2010, 53, 6730–6746. [PubMed: 20718423]
- (25). Singh V; Evans GB; Lenz DH; Mason JM; Clinch K; Mee S; Painter GF; Tyler PC; Furneaux RH; Lee JE; Howell PL; Schramm VL Femtomolar Transition State Analogue Inhibitors of 5′-Methylthioadenosine/S-Adenosylhomocysteine Nucleosidase from *Escherichia coli*. *J. Biol. Chem* 2005, 280, 18265–18273. [PubMed: 15749708]
- (26). Evans GB; Furneaux RH; Schramm VL; Singh V; Tyler PC Targeting the Polyamine Pathway with Transition-State Analogue Inhibitors of 5′-Methylthioadenosine Phosphorylase. *J. Med. Chem* 2004, 47, 3275–3281. [PubMed: 15163207]
- (27). Singh V; Schramm VL Transition-State Analysis of *S. pneumoniae* 5′-Methylthioadenosine Nucleosidase. *J. Am. Chem. Soc* 2007, 129, 2783–2795. [PubMed: 17298059]
- (28). Namanja-Magliano HA; Stratton CF; Schramm VL Transition State Structure and Inhibition of Rv0091, a 5′-Deoxyadenosine/5′-methylthioadenosine Nucleosidase from *Mycobacterium tuberculosis*. *ACS Chem. Biol* 2016, 11, 1669–1676. [PubMed: 27019223]
- (29). Singh V; Shi W; Evans GB; Tyler PC; Furneaux RH; Almo SC; Schramm VL Picomolar Transition State Analogue Inhibitors of Human 5′-Methylthioadenosine Phosphorylase and XRay Structure with MT-Immucillin-A. *Biochemistry* 2004, 43, 9–18. [PubMed: 14705926]
- (30). Evans GB; Furneaux RH; Schramm VL; Singh V; Tyler PC Targeting the Polyamine Pathway with Transition-State Analogue Inhibitors of 5′-Methylthioadenosine Phosphorylase. *J. Med. Chem* 2004, 47, 3275–3281. [PubMed: 15163207]
- (31). Kicska GA; Tyler PC; Evans GB; Furneaux RH; Shi W; Fedorov A; Lewandowicz A; Cahill SM; Almo SC; Schramm VL Atomic Dissection of the Hydrogen Bond Network for Transition-State Analogue Binding to Purine Nucleoside Phosphorylase. *Biochemistry* 2002, 41, 14489–14498. [PubMed: 12463747]
- (32). Evans GB; Furneaux RH; Lewandowicz A; Schramm VL; Tyler PC Synthesis of Second-Generation Transition State Analogues of Human Purine Nucleoside Phosphorylase. *J. Med. Chem* 2003, 46, 5271–5276. [PubMed: 14613329]
- (33). Rostovtsev VV; Green LG; Fokin VV; Sharpless KB A Stepwise Huisgen Cycloaddition Process: Copper (I)-Catalyzed Regioselective “Ligation” of Azides and Terminal Alkynes. *Angew. Chem* 2002, 114, 2708–2711.
- (34). Evans GB; Cameron SA; Luxenburger A; Guan R; Suarez J; Thomas K; Schramm VL; Tyler PC Tight Binding Enantiomers of Pre-Clinical Drug Candidates. *Bioorg. Med. Chem* 2015, 23, 5326–5333. [PubMed: 26260335]
- (35). McCoy AJ; Grosse-Kunstleve RW; Adams PD; Winn MD; Storoni LC; Read RJ Phaser Crystallographic Software. *J. Appl. Crystallogr* 2007, 40, 658–674. [PubMed: 19461840]
- (36). Chen VB; Arendall WB 3rd; Headd JJ; Keedy DA; Immormino RM; Kapral GJ; Murray LW; Richardson JS; Richardson DC MolProbity: All-Atom Structure Validation for Macromolecular Crystallography. *Acta Crystallogr., Sect. D: Biol. Crystallogr* 2010, 66, 12–21. [PubMed: 20057044]
- (37). Kim RQ; Offen WA; Davies GJ; Stubbs KA Structural Enzymology of *Helicobacter pylori* Methylthioadenosine Nucleosidase in the Futasoline Pathway. *Acta Crystallogr., Sect. D: Biol. Crystallogr* 2014, 70, 177–185. [PubMed: 24419390]
- (38). Mishra V; Ronning DR Crystal Structures of the *Helicobacter pylori* MTAN Enzyme Reveal Specific Interactions between S-Adenosylhomocysteine and the 5′-Alkylthio Binding Subsite. *Biochemistry* 2012, 51, 9763–9772. [PubMed: 23148563]
- (39). Ronning DR; Iacopelli NM; Mishra V Enzyme-Ligand Interactions That Drive Active Site Rearrangements in the *Helicobacter pylori* 5′-Methylthioadenosine/S-Adenosylhomocysteine Nucleosidase. *Protein Sci* 2010, 19, 2498–2510. [PubMed: 20954236]

- (40). Appleby TC; Erion MD; Ealick SE The Structure of Human 5'-Deoxy-5'-Methylthioadenosine Phosphorylase at 1.7 Å Resolution Provides Insights into Substrate Binding and Catalysis. *Structure* 1999, 7, 629–641. [PubMed: 10404592]
- (41). Guan R; Ho M-C; Brenowitz M; Tyler PC; Evans GB; Almo SC; Schramm VL Entropy-Driven Binding of Picomolar Transition State Analogue Inhibitors to Human 5'-Methylthioadenosine Phosphorylase. *Biochemistry* 2011, 50, 10408–10417. [PubMed: 21985704]
- (42). Lee JE; Cornell KA; Riscoe MK; Howell PL Structure of E. coli 5'-Methylthioadenosine/S-Adenosylhomocysteine Nucleosidase Reveals Similarity to the Purine Nucleoside Phosphorylases. *Structure* 2001, 9, 941–953. [PubMed: 11591349]
- (43). Lee JE; Smith GD; Horvatin C; Huang DJT; Cornell KA; Riscoe MK; Howell PL Structural Snapshots of MTA/AdoHcy Nucleosidase Along the Reaction Coordinate Provide Insights into Enzyme and Nucleoside Flexibility During Catalysis. *J. Mol. Biol* 2005, 352, 559–574. [PubMed: 16109423]
- (44). Banco MT; Mishra V; Ostermann A; Schrader TE; Evans GB; Kovalevsky A; Ronning DR Neutron Structures of the *Helicobacter pylori* 5'-Methylthioadenosine Nucleosidase Highlight Proton Sharing and Protonation States. *Proc. Natl. Acad. Sci. USA* 2016, 113, 13756–13761. [PubMed: 27856757]
- (45). Morrison JF; Walsh CT The Behavior and Significance of Slow-Binding Enzyme Inhibitors. *Adv. Enzymol. Relat. Areas Mol. Biol* 1988, 61, 201–301. [PubMed: 3281418]
- (46). Battye TG; Kontogiannis L; Johnson O; Powell HR; Leslie AG IMOSFLM: A New Graphical Interface for Diffraction-Image Processing with MOSFLM. *Acta Crystallogr., Sect. D: Biol. Crystallogr* 2011, 67, 271–281. [PubMed: 21460445]
- (47). Collaborative Computational Project, N. 4. The CCP4 Suite: Programs for Protein Crystallography. *Acta Crystallogr., Sect. D: Biol. Crystallogr* 1994, 50, 760–763. DOI: 10.1107/S0907444994003112. [PubMed: 15299374]
- (48). Adams PD; Afonine PV; Bunkoczi G; Chen VB; Davis IW; Echols N; Headd JJ; Hung LW; Kapral GJ; Grosse-Kunstleve RW; McCoy AJ; Moriarty NW; Oeffner R; Read RJ; Richardson DC; Richardson JS; Terwilliger TC; Zwart PH PHENIX: A Comprehensive Python-Based System for Macro-molecular Structure Solution. *Acta Crystallogr., Sect. D: Biol. Crystallogr* 2010, 66, 213–221. [PubMed: 20124702]
- (49). Emsley P; Lohkamp B; Scott WG; Cowtan K Features and Development of Coot. *Acta Crystallogr., Sect. D: Biol. Crystallogr* 2010, 66, 486–501. [PubMed: 20383002]
- (50). Murshudov GN; Vagin AA; Dodson EJ Refinement of Macromolecular Structures by the Maximum-Likelihood Method. *Acta Crystallogr., Sect. D: Biol. Crystallogr* 1997, 53, 240–255. [PubMed: 15299926]

**Figure 1.**

Transition states and reactions catalyzed by MTAP and *Hp*MTAN. (A) MTAP catalyzes the reaction via a ribocationic transition state and phosphate as the nucleophile. Adenine and methylthio- α -D-ribose 1-phosphate are the products. Bonds to the leaving group and the attacking nucleophile are weak, less than 0.1 Pauling bond order, making the reaction more S_N1 than S_N2 in character. (B) *Hp*MTAN also catalyzes its reaction via a ribocationic transition state. Water acts as the nucleophile. Adenine and methylthio-D-ribose are the products.

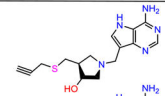
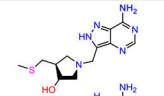
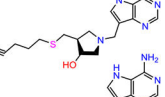
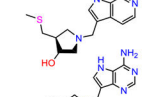
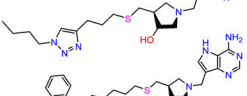
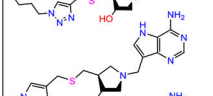
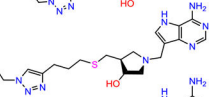
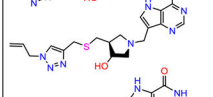
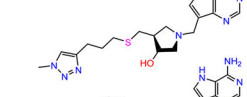
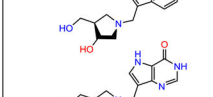
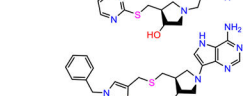
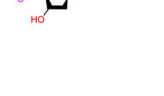


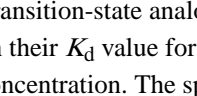
Code	Inhibitor	K_d (nM)			Code	Inhibitor	K_d (nM)		
		HsMTAP	HpMTAN	K_d Hs/Hp			HsMTAP	HpMTAN	K_d Hs/Hp
15		0.63 ± 0.08	0.055 ± 0.025	11.5	11		19 ± 1.5	0.235 ± 0.064	80.9
16		0.94 ± 0.12	0.026 ± 0.006	36.2	8		31.9 ± 7.9	10.3 ± 1.9	3.1
30		1.3 ± 0.1	0.028 ± 0.010	46.4	29		37 ± 7.0	0.373 ± 0.135	99.2
32		1.4 ± 0.1	0.036 ± 0.010	38.9	25		66 ± 6.6	0.274 ± 0.096	241
28		2.4 ± 0.3	0.026 ± 0.005	92.3	27		70 ± 3.2	0.288 ± 0.023	243
26		3.0 ± 0.2	0.025 ± 0.002	120	34		ND	ND	
33		13 ± 4.8	0.058 ± 0.006	224	35		ND	ND	
31		13 ± 1.4	0.073 ± 0.021	178					

Figure 2. Transition-state analogue inhibitors of MTAP and *Hp*MTAN. Inhibitors were ranked based on their K_d value for MTAP. ND means inhibition not detected at a 5 μ M inhibitor concentration. The specificity ratio (K_d Hs/Hp) is the affinity for human MTAP relative to *Hp*MTAN.

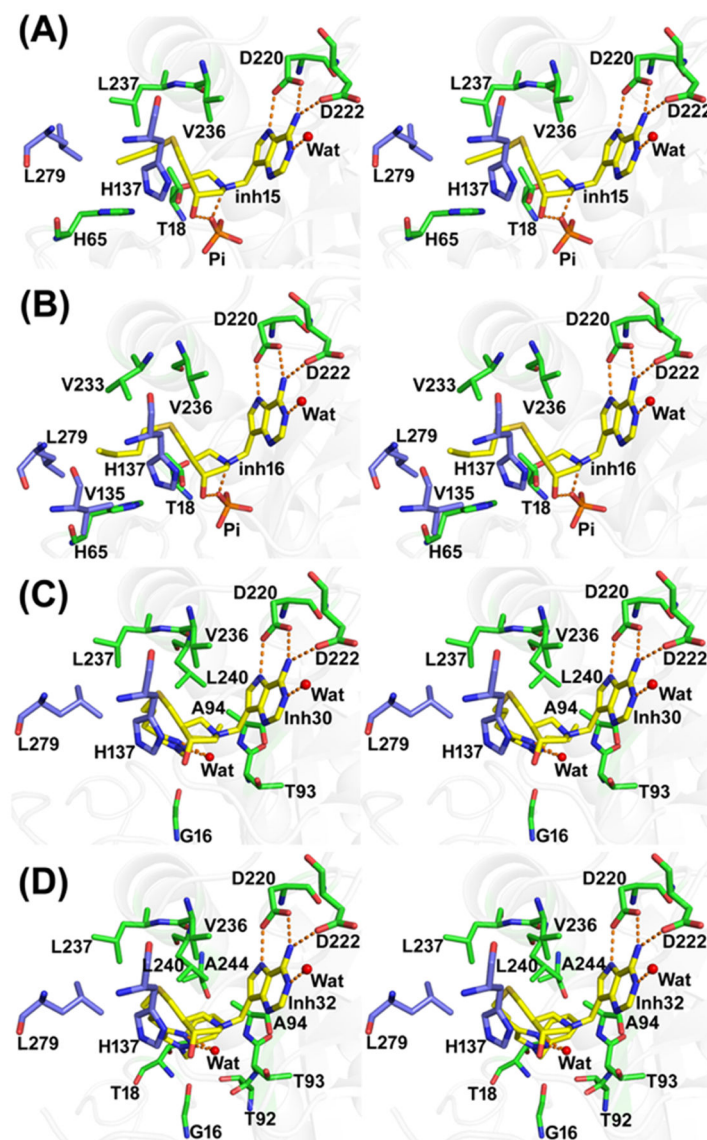


Figure 3. Stereoview of the binding sites of MTAP in complex with transition-state analogue inhibitors. The inhibitor complexes of **15**, **16**, **30**, and **32** are shown in panels A, B, C, and D, respectively. The residues interacting with inhibitors from monomer-A are shown in green and from the neighboring subunit are shown in light blue. Selected hydrogen bond interactions are shown in orange dotted lines.

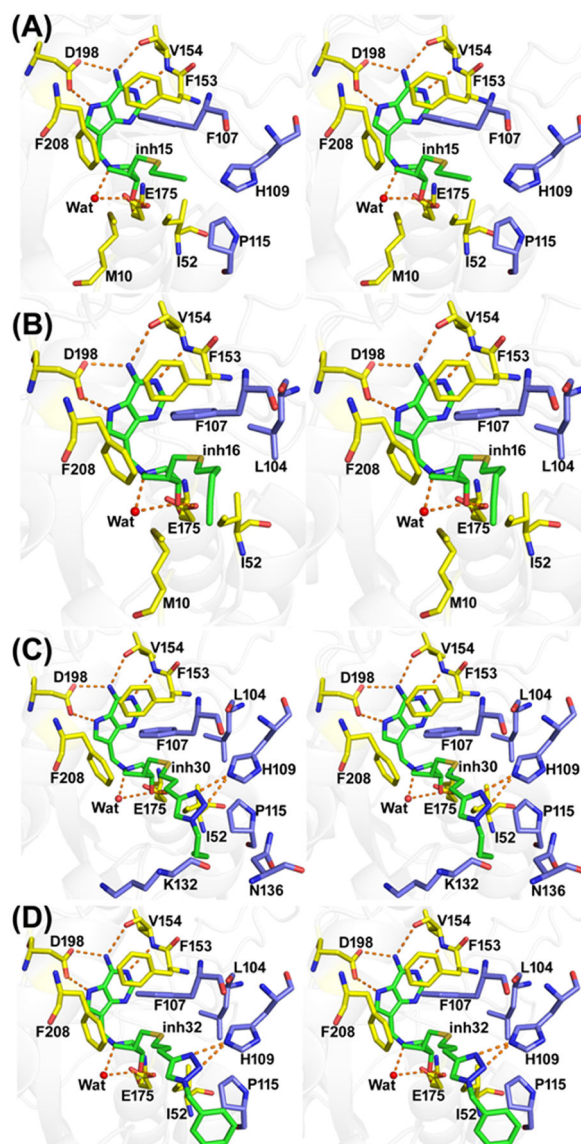


Figure 4. Stereoview of the binding sites of *HpMTAN* in complex with transition-state analogue inhibitors. The inhibitor complexes of **15**, **16**, **30**, and **32** are shown in panels A, B, C, and D, respectively. The residues interacting with inhibitors from monomer-A are shown in yellow and from monomer-B are shown in light blue. Selected hydrogen bond interactions are shown in orange dotted lines.

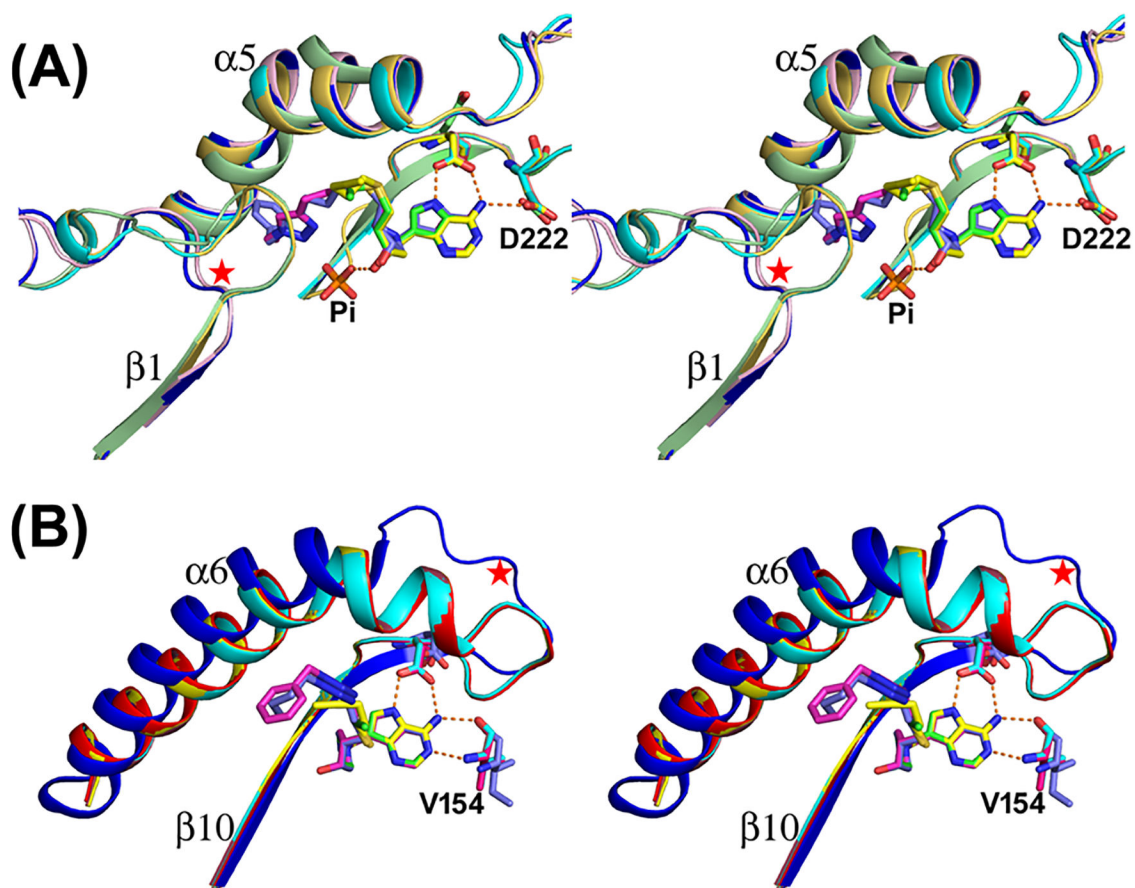
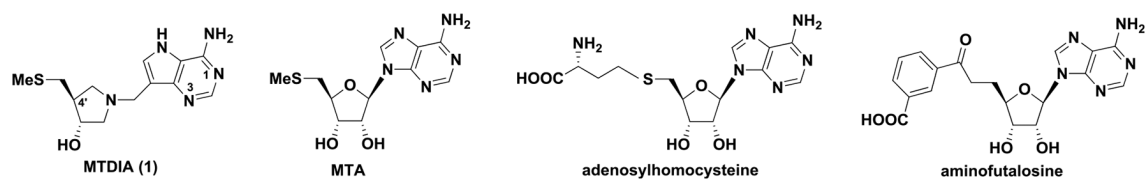
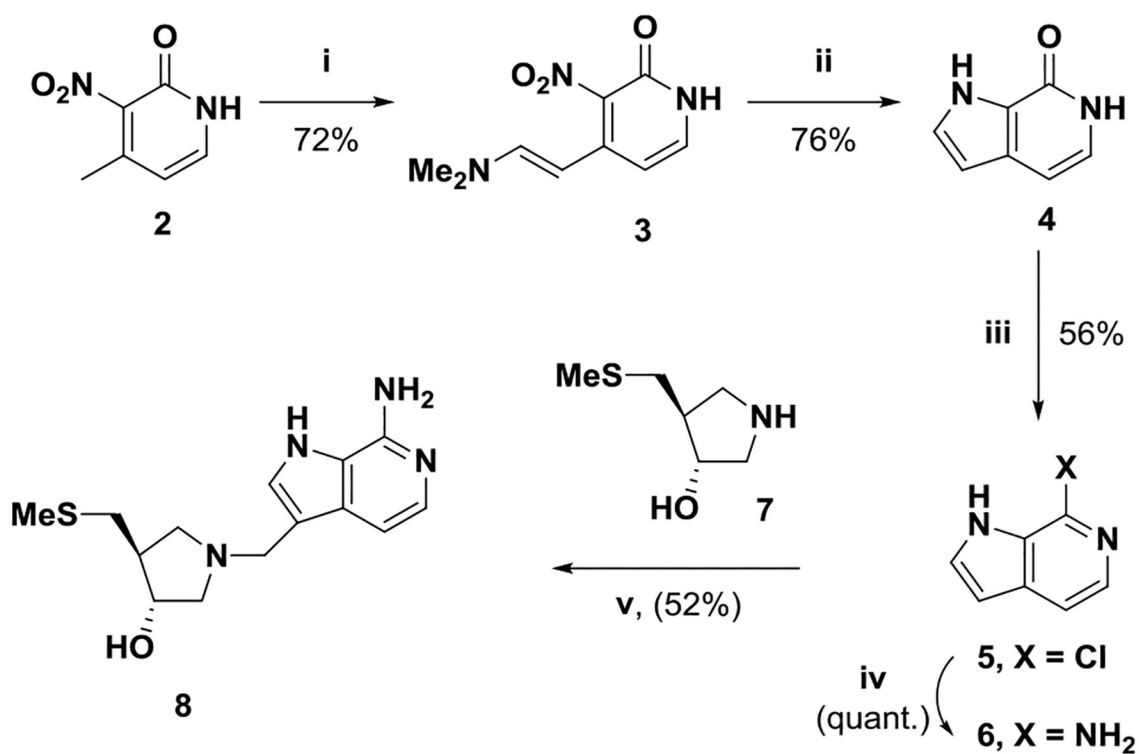


Figure 5. Catalytic site conformations of apo- and ligand-bound MTAP and *Hp*MTAN. (A) Stereoview superposition of unliganded MTAP (PDB ID: 3OZE; green) with four inhibitor-bound structures, including MTAP-15 (PDB ID: 6DYZ; cyan), MTAP-16 (PDB ID: 6DZ0; yellow), MTAP-30 (PDB ID: 6DZ3; blue), and MTAP-32 (PDB ID: 6DZ2; light pink), are overlapped. The $\beta 1$ – $\beta 2$ loop (highlighted with a red star) is altered substantially on the binding of **30** and **32**. (B) Superposition of an unliganded MTAN binding site (*E. coli* MTAN PDB ID: 1Z5P; blue) with four inhibitor-bound complexes of *Hp*MTAN, including MTAN-15 (PDB ID: 6DYU; brick red), MTAN-16 (PDB ID: 6DYV; cyan), MTAN-30 (6DY Y; yellow), and MTAN-32 (6DY W; red). Helix 6 and associated loop of the unliganded MTAN change conformation to elongate helix 6 as a result of inhibitor binding (highlighted with a red star).

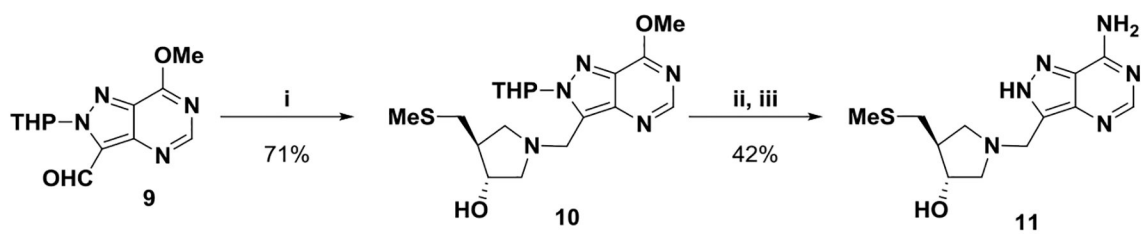


Scheme 1.

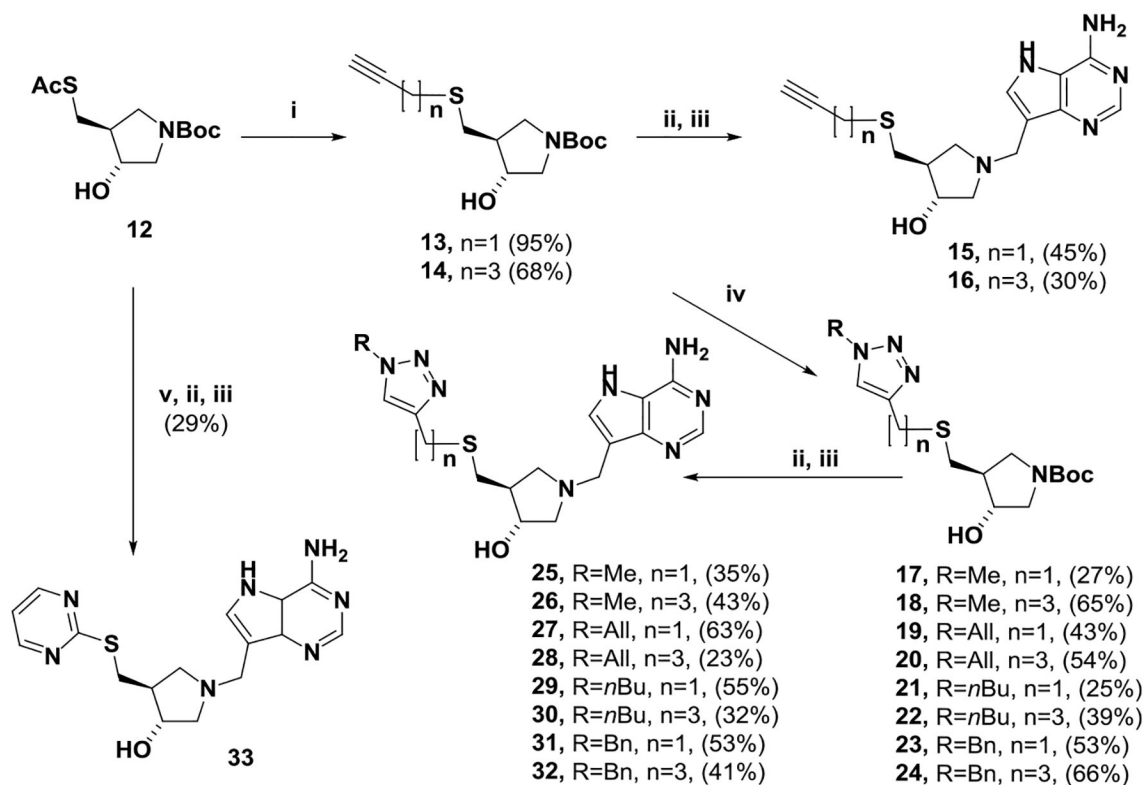


Scheme 2.

Reagents: (i) *t*BuOCH(NMe₂)₂, DMF, 100 °C; (ii) Zn, HOAc; (iii) POCl₃ 100 °C; (iv) aq NH₃, CuCl, 120 °C; and (v) HCHO, aq EtOH, 80–100 °C

**Scheme 3.**

Reagents: (i) Picoline Borane, 7, MeOH; (ii) 7 N NH₃/MeOH, 120 °C; and (iii) aq HCl, MeOH



Scheme 4.

HCl (conc.) 3:1 v/v; (iii) 9-Deazaadenine, Formaldehyde, EtOH/Water, 70–100 °C (Microwave), 2–6 h; (iv) MeI, Allyl Bromide, *n*BuBr or BnBr, NaN₃, CuI, MeOH; and (v) NaOMe, MeOH, and then 2-Chloropyrimidine

Table 1.

Data Collection and Refinement Statistics of MTAP and HpMTAN Complexes

Dataset ^a	<i>H. sapiens</i> MTAP						<i>H. pylori</i> MTAN					
	MTAP + 15	MTAP + 16	MTAP + 30	MTAP + 32	HpMTAN + 15	HpMTAN + 16	HpMTAN + 30	HpMTAN + 32				
space group	<i>P</i> 321	<i>P</i> 321	<i>C</i> 222 ₁	<i>C</i> 222 ₁	<i>P</i> 4 ₁ 2 ₁ 2	<i>P</i> 4 ₁ 2 ₁ 2	<i>P</i> 2 ₁ 2 ₁ 2 ₁	<i>P</i> 4 ₁ 2 ₁ 2				
cell parameters (Å, deg)	<i>a</i> = 122.82 <i>b</i> = 122.82 <i>c</i> = 44.62 <i>α, β, γ</i> = 90, <i>γ</i> = 120.0	<i>a</i> = 121.81 <i>b</i> = 121.81 <i>c</i> = 44.37 <i>α, β, γ</i> = 90, <i>γ</i> = 120	<i>a</i> = 79.36 <i>b</i> = 135.13, <i>c</i> = 158.86 <i>α, β, γ</i> = 90	<i>a</i> = 79.39, <i>b</i> = 135.32 <i>c</i> = 159.27 <i>α, β, γ</i> = 90	<i>a</i> = 73.25 <i>b</i> = 73.25 <i>c</i> = 176.14 <i>α, β, γ</i> = 90	<i>a</i> = 73.48 <i>b</i> = 73.48 <i>c</i> = 176.21 <i>α, β, γ</i> = 90	<i>a</i> = 73.25 <i>b</i> = 73.25 <i>c</i> = 176.14 <i>α, β, γ</i> = 90	<i>a</i> = 72.56 <i>b</i> = 74.03 <i>c</i> = 176.89 <i>α, β, γ</i> = 90	<i>a</i> = 73.35 <i>b</i> = 73.35 <i>c</i> = 176.38 <i>α, β, γ</i> = 90			
<i>V_m</i> (Å ³ /Dalton)	2.9	2.9	2.2	2.2	2.2	2.2	2.2	2.2				
number of subunits in the asymmetric unit	1	1	3	3	2	2	4	2				
Data Collection												
beamline	LRL-CAT	LRL-CAT	LRL-CAT	LRL-CAT	LRL-CAT	LRL-CAT	LRL-CAT	LRL-CAT				
wavelength (Å)	0.97931	0.97931	0.97931	0.97931	0.97931	0.97931	0.97931	0.97931				
temperature (K)	100	100	100	100	100	100	100	100				
resolution range (Å)	53.18–1.62 (1.65–1.62)	60.91–1.62 (1.65–1.62)	79.43–1.91 (1.95–1.91)	79.63–1.99 (2.04–1.99)	67.64–1.60 (1.63–1.60)	88.10–1.62 (1.65–1.62)	176.89–1.61 (1.64–1.61)	88.19–1.45 (1.47–1.45)				
total number of observed reflections	605 199 (28 477)	600 969 (27711)	497 405 (33 410)	438 725 (30 921)	927 868 (45 362)	852 192 (25 016)	912 840 (44 290)	1242 406 (60 058)				
number of unique reflections	48 526 (2329)	48 221 (2355)	66 387 (4430)	59 017 (4097)	64 250 (3121)	61 452 (2548)	123 910 (5998)	86 142 (4167)				
<i>R_{merge}</i> (%) ^b	9.8 (121.8)	11.0 (133.5)	9.4 (109.3)	10.0 (116.2)	14.6 (152.8)	11.5 (109.4)	9.9 (99.1)	14.9 (175.4)				
<i>R_{rim}</i> (%) ^c	2.9 (36.0)	3.2 (40.3)	3.7 (42.6)	3.9 (45.0)	4.0 (41.3)	3.1 (34.9)	3.9 (39.0)	4.1 (47.5)				
CC1/2 (%)	99.9 (75.8)	99.9 (71.4)	99.8 (70.2)	99.9 (72.5)	99.9 (69.8)	99.8 (69.6)	99.7 (80.2)	99.7 (76.0)				
<i>I</i> (<i>σ</i> (<i>I</i>)) ^d	18.3 (2.0)	14.9 (2.0)	13.0 (1.9)	13.4 (1.9)	13.8 (2.0)	14.8 (2.0)	11.4 (2.1)	11.2 (2.0)				
completeness (%)	98.6 (96.3)	100 (100)	99.9 (100)	99.9 (100)	100 (99.9)	98.7 (84.0)	100 (100)	100 (100)				
multiplicity	12.5 (12.2)	12.5 (11.8)	7.5 (7.5)	7.4 (7.5)	14.4 (14.5)	13.9 (9.8)	7.4 (7.4)	14.4 (14.4)				
Wilson B-factor (Å ²)	15.5	15.5	27.2	35.2	15.1	14.7	16.7	13.2				
Refinement												
<i>R_{work}</i> (%) ^e	16.9	15.5	19.7	20.1	16.4	16.7	18.0	17.7				
<i>R_{free}</i> (%) ^f	19.0	17.6	22.2	23.6	19.3	19.3	20.3	20.0				

Dataset ^d	<i>H. sapiens</i> MTAP				<i>H. pylori</i> MTAN			
	MTAP + 15	MTAP + 16	MTAP + 30	MTAP + 32	HpMTAN + 15	HpMTAN + 16	HpMTAN + 30	HpMTAN + 32
no. of atoms	2444	2428	6758	6615	4208	4152	8152	4168
protein atoms	2137	2132	6290	6199	3596	3587	7104	3568
ligand atoms	22	24	93	102	44	48	124	68
solvent atoms	285	272	375	314	568	517	924	532
Model Quality								
RMS Deviation from Ideal Value								
bond length (Å)	0.011	0.011	0.009	0.01	0.01	0.01	0.01	0.009
bond angle (deg)	1.6	1.6	1.6	1.6	1.5	1.6	1.7	1.6
Average B-Factor								
protein atoms (Å ²)	21.6	22.3	38.3	43.8	17.7	20.6	23.3	18.8
ligand atoms (Å ²)	16.4	17.3	41.0	46.1	13.3	15.5	23.1	21.0
waters (Å ²)	36.1	36.5	40.1	42.1	31.5	33.3	34.5	31.5
Ramachandran plot^g								
most favored regions (%)	97.5	98.2	97.7	98.0	97.1	96.9	97.0	96.6
allowed regions (%)	2.5	1.8	1.7	2.0	2.9	3.1	3.0	3.4
outlier regions (%)	0.0	0.0	0.6	0.0	0.0	0.0	0.0	0.0
PDB ID entry	6DYZ	6DZ0	6DZ3	6DZ2	6DYU	6DYY	6DYY	6DYYW

^aValues in parentheses refer to the highest resolution shell.

^b $R_{\text{merge}} = \frac{\sum \langle |I(hkl) - \langle I(hkl) \rangle| \rangle}{\sum I(hkl)}$, where $I(hkl)$ is the intensity of the h th measurement of reflection (hkl) and $\langle I(hkl) \rangle$ is its mean intensity.

^c $R_{\text{pim}} = \frac{\sum \langle |I(hkl) - \langle I(hkl) \rangle| \rangle}{\sum I(hkl)}$, where $I(hkl)$ is the intensity of the i th measurement of reflection (hkl) , $\langle I(hkl) \rangle$ is its mean intensity, and N is the number of measurements.

^d σ_I is the integrated intensity and $\sigma(I)$ is its estimated standard deviation.

^e $R_{\text{work}} = \frac{\sum \langle |F_o - F_c| \rangle}{\sum F_o}$, where F_o and F_c are the observed and calculated structural factors.

^f R_{free} is calculated as for R_{work} but from a randomly selected subset of the data (5%), which were excluded from the refinement calculation.

^gCalculated by MOLPROBITY.

Table 2.Amino Acid Residues in Contact with the 5'-Alkylthio Groups of Transition-State Analogue Inhibitors^a

inhibitors	MTAP	HpMTAN
15	Thr18, His65, Val236, Leu237, His137*, Leu279*	Met10, Ile52, Phe153, Phe208, Phe107*, His109*, Pro115*
16	Thr18, His65, Val233, Val236, Val135*, His137*, Leu279*	Met10, Ile52, Phe153, Phe208, Leu104*, Phe107*
30	Gly16, Thr93, Ala94, Val236, Leu237, Leu240, His137*, Leu279*	Ile52, Phe153, Phe208, Leu104*, Phe107*, His109*, Pro115*, Lys132*, Asn136*
32	Gly16, Thr18, Thr92, Thr93, Ala94, Val236, Leu237, Leu240, Ala244, His137*, Leu279*	Ile52, Phe153, Phe208, Leu104*, Phe107*, His109*, Pro115*

^a Amino acids interacting within the 5'-alkylthio pocket (to 3.9 Å) are reported. These residues interacting from the neighboring subunits are highlighted with an asterisk (*).